Chin. J. Astron. Astrophys. Vol. 3 (2003), No. 2, 133–141
(http://www.chjaa.org or http://chjaa.bao.ac.cn)

Chinese Journal of
Astronomy and
Astrophysics

A Kinematical Study of the NGC 7538 IRS 1 Region *

Ye Xu [1,2,3], Xing-Wu Zheng [2] and Dong-Rong Jiang [3]

[1] National Astronomical Observatories, Chinese Academy of Sciences, Urumqi 830011; xuye@nju.edu.cn

[2] Department of Astronomy, Nanjing University, Nanjing 210093

[3] Shanghai Astronomical Observatory, Chinese Academy of Sciences, Shanghai 200030

Received 2002 September 20; accepted 2002 December 30

Abstract We present high angular resolution images of both NH_3 (1, 1) and (2, 2) lines toward NGC 7538 IRS 1. The density and velocity-position plots have been used to study the interaction among the outflows, winds and their environment. For the first time we have found an expanding half-shell of molecular gas around the HII region associated with IRS 1, which may be produced by the interaction of the bipolar outflows and the winds originating in IRS 1–3, and optical HII region NGC 7538 with ambient molecular gas.

Key words: HII regions — ISM: clouds — ISM: individual (NGC 7538) — ISM: kinematics

1 INTRODUCTION

NGC 7538 is one of the most studied regions of star formation in the Galaxy. At a distance of 3 kpc, the NGC 7538 complex has been the object of numerous optical, infrared, and radio observations. The complex consists of an optically visible HII region and at least three compact infrared components, IRS 1–3. The component IRS 1 is an ultra-compact HII region in the radio continuum.

A bipolar CO outflow was detected toward NGC 7538 IRS 1 (Scoville et al. 1986; Davis et al. 1998). Several molecular masers were detected toward IRS 1, such as OH (Dickel et al. 1982), H_2O (Kameya et al. 1990), CH_3OH (Menten et al. 1986), H_2CO (Rots et al. 1981), NH_3 (Madden et al. 1986), and $^{15}NH_3$ (Gaume et al. 1991). Scoville et al. (1986) and Pratap, Snyder & Batrla (1992) found a rotating ^{13}CO structure, centered on IRS 1, which may help to constrain the expansion of the HII region. Interferometric imaging of quasi-thermal molecular emission was made for ^{13}CO, HCO^+ (Pratap, Snyder & Batrla 1992), which showed the presence of a cavity in the material around the IRS 1 HII region. The presence of ^{13}CO emission and the absence of HCO^+ emission in the cavity would imply densities between $\sim 10^3$ and $10^5\,cm^{-3}$.

* Supported by the National Natural Science Foundation of China.

These studies indicate a complex spatial and kinematic distribution of molecular material in the vicinity of NGC 7538 IRS 1 with an average local standard of rest (LSR) velocity in the range –53 to –67 km s^{-1}.

NH_3 lines have been proved to be excellent tracers of the dense molecular gas around newly formed stars. Zheng et al. (2001) observed the $(J, K) = (1, 1)$ and (2, 2) inversion lines of NH_3 at 23694.495 and 23722.633 MHz toward NGC 7538 using the VLA in 1990 and 1995, and obtained the density, temperature and velocity position structures across the whole NGC 7538 region. However, they have not yet studied the kinematic structure in detail in some active star-forming areas, such as NGC 7538 IRS 1 region which may have an important impact on the evolution of NGC 7538 as a whole. To better understand the physical conditions and kinematics of dense and hot molecular cores associated with NGC 7538 IRS 1 region, we have re-reduced these data using the NRAO AIPS (Astronomical Image Processing System) package. For the first time we have found an expanding half-shell of molecular gas around the HII associated with IRS 1.

2 RESULTS

2.1 NH_3 Emission

Figure 1 shows NH_3 integrated maps for the (1, 1) line toward IRS 1, integrated over the range from –54.1 to –60.3 km s^{-1}. The NH_3 spectra show absorption projected against the

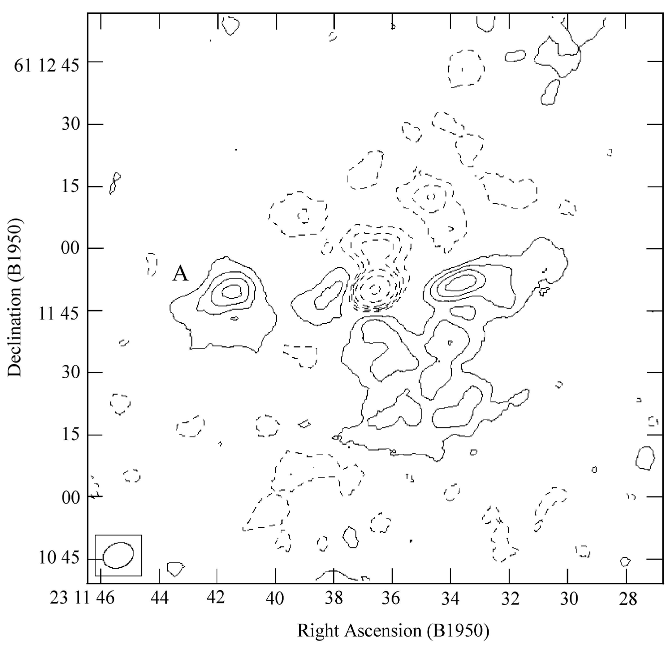

Fig. 1 Contours show the integrated intensity (moment zero) of the central component of the (1, 1) line transition, integrated from –54.1 to –60.3 km s^{-1}. The contours are plotted at –1.1, –0.55, –0.28, –0.15, –0.11, –0.06, 0.06, 0.11, 0.15, and 0.22 Jy $beam^{-1} \times$ km s^{-1}.

IRS 1 HII region, while emission forms a half-ring shape around the HII region. It is notable that there is a gap between the absorption and the emission. Absorption arises in opaque lines only when the continuum brightness exceeds the line brightness temperature, and if, on the contrary, the former is less than the latter, emission line would be expected. The lack of both absorption and emission in the gap is most likely because of the approximate equality between the continuum brightness and the line brightness temperature. In addition, some faint lines might not be detected in the gap due to the inadequate signal-to-noise ratio. One can see that a possible geometry for the molecular material is a shell or ring: the absorption arises from the top of the shell or center of the ring, while the emission comes from the projection of the half-shell or half-ring in the south.

Figure 2 shows the NH_3 absorption spectra at (1, 1) and (2, 2) transitions toward IRS 1. The wide bandpass in this observation covers the main and satellite lines. The inner satellites are separated from the main hyperfine component by $\sim$7.8 km s^{-1}, and 16.4 km s^{-1} for (1, 1) and (2, 2) transitions, respectively. Our high-resolution measurements provide a good opportunity to study the shape of the absorption components. In the (1, 1) transition, the main and the inner pair of the satellite components are blended, while in the (2, 2) transition, the satellite lines are completely resolved from the main line owing to large splittings and so there is no confusion among the five components.

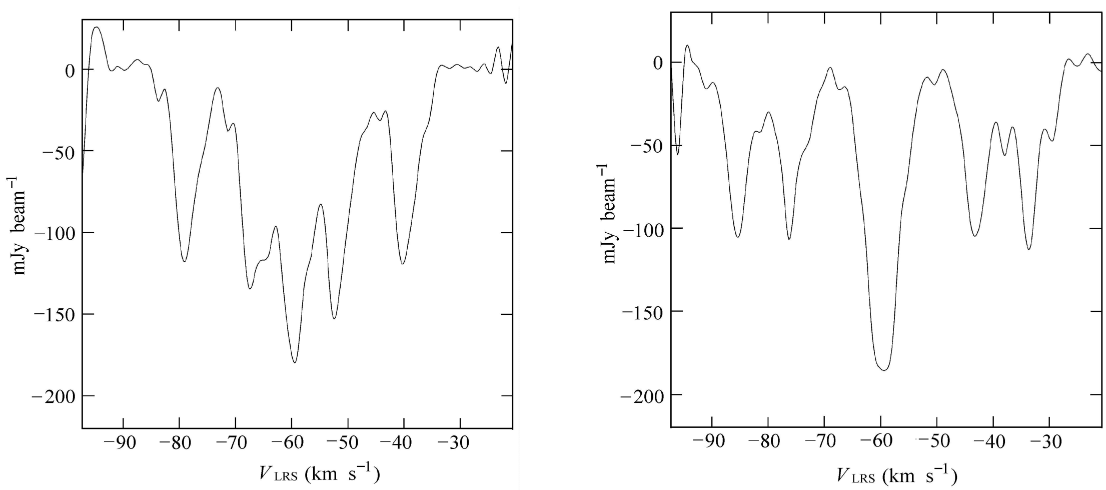

Fig. 2 Absorption spectra of the (1, 1) line (left) and (2, 2) (right) line toward the HII region associated with IRS 1. The velocity resolution is 1.24 km s^{-1}. The rms noise is 6 mJy per beam.

Hyperfine structures in the NH_3 spectra allow us to determine the optical depths (Ho & Haschick 1986), according to relation

$$\frac{\Delta T_a^*(J,K,m)}{\Delta T_a^*(J,K,s)} = \frac{1-e^{-\tau(J,K,m)}}{1-e^{-a\tau(J,K,m)}}, \tag{1}$$

where m and s refer to the main and satellite components, ΔT_a^* is the measured brightness temperature, and $\tau(J,K,m)$ is the optical depth of the main component. For the (1, 1) outer pair of the satellite components, $a = 0.22$ (Wilson et al. 1978). From Figure 2, we measured the line emission with –173 mJy beam^{-1} and –176 mJy beam^{-1} for the (1, 1) and the (2, 2) main component, respectively, and 120 mJy beam^{-1} and 107 mJy beam^{-1} for the (1, 1) and (2, 2) satellite components, respectively. Hence, we derived an average optical depth of 5.1 for the (1, 1) line and 13.4 for the (2, 2) line with an uncertainty of 10%.

The apparent optical depth, defined as the ratio of the line intensity to the continuum flux, can be expressed as (Wilson et al. 1978)

$$\tau_{\rm apparent} = -\ln\left(1 - \frac{|T_L|}{T_c}\right) . \tag{2}$$

From Figure 3, we measured the continuum emission with 317 mJy beam^{-1} at 23.69 GHz, and 316 mJy beam^{-1} at 23.72 GHz. From Equation (2), we estimated apparent optical depths of 0.84 and 0.88 respectively. The difference in optical depth may indicate that the molecular material projected against the background continuum source is very clumpy (Wilson et al. 1978).

Because the spectra have a poor signal-to-noise ratio in the emission lines, we could not easily obtain the optical depth of most regions around IRS 1. However, we could distinguish the main and satellite components in an ammonia clump, marked A in Figures 1 and 4. In this region, we measured a (1, 1) main line intensity of 74.5 mJy beam^{-1} and an inner satellite line intensity of 24.5 mJy beam^{-1}. Thus we derived an average optical depth of 0.69.

An approximate rotational temperature can be deduced by observing the inversion transitions of two rotational states, such as the (1, 1) and (2, 2) lines (Wiseman & Ho 1998)

$$T_R(2,2;1,1) = -41.5 \div \ln\left\{\frac{-0.282}{\tau_m(1,1)} \ln\left[1 - \frac{\Delta T_a^*(2,2,m)}{\Delta T_a^*(1,1,m)}(1 - e^{-\tau_m(1,1)})\right]\right\} . \tag{3}$$

From Figure 4 we measured an intensity of 43.5 mJy beam^{-1} for the (2, 2) main line. Assuming equal excitation temperatures and using the previously determined values of the line opacities, we obtained a rotational temperature of 21 K for the emission gas, T_R.

We can also estimate the column density of NH_3 from the optical depth of an inversion transition, $\tau_{(J,K)}$, and the excitation temperature, $T_{\rm ex}$, using the expression (Wiseman & Ho 1998)

$$N({\rm NH_3}) \approx 1.7 \times 10^{15}{\rm cm}^{-2}\left[\frac{J\nu(T_{\rm ex})}{20\,{\rm K}}\right]\left[\frac{\tau_{(J,K)}}{1}\right]\left[\frac{\Delta V}{2\ {\rm km\,s^{-1}}}\right]\left[\frac{f_{J,K}}{0.3}\right]^{-1}, \tag{4}$$

where J$\nu(T_{\rm ex})$ is the flux intensity in temperature units, ΔV is the line width in units of km s^{-1} and $f_{J,K}$ is the fractional population in the (J,K) state. Assuming $J\nu(T_{\rm ex}) = 20$ K and $f_{J,K} \approx 0.43$ (Wiseman & Ho 1998), and the observed line width of ~ 2.3 km s^{-1} in the region A in Figure 4, we obtained $N({\rm NH_3}) \simeq 1.3 \times 10^{15}$ cm^{-2}.

By assuming a core density distribution and the abundance fraction of NH_3 relative to H_2, the mass of the core can be calculated. For a simple uniform sphere, the density n and mass M are approximately (Wiseman & Ho 1998)

$$n \simeq 4.4 \times 10^3\,{\rm cm}^{-3}\left[\frac{N({\rm NH_3})}{10^{15}\,{\rm cm}^{-2}}\right]\left[\frac{A}{1\,{\rm pc}^2}\right]^{-1/2}\left[\frac{n({\rm NH_3})/n({\rm H_2})}{10^{-7}}\right]^{-1}, \tag{5}$$

and

$$M \simeq 160 M_\odot\left[\frac{N({\rm NH_3})}{10^{15}\,{\rm cm}^{-2}}\right]\left[\frac{A}{1\,{\rm pc}^2}\right]^{-1/2}\left[\frac{n({\rm NH_3})/n({\rm H_2})}{10^{-7}}\right]^{-1}. \tag{6}$$

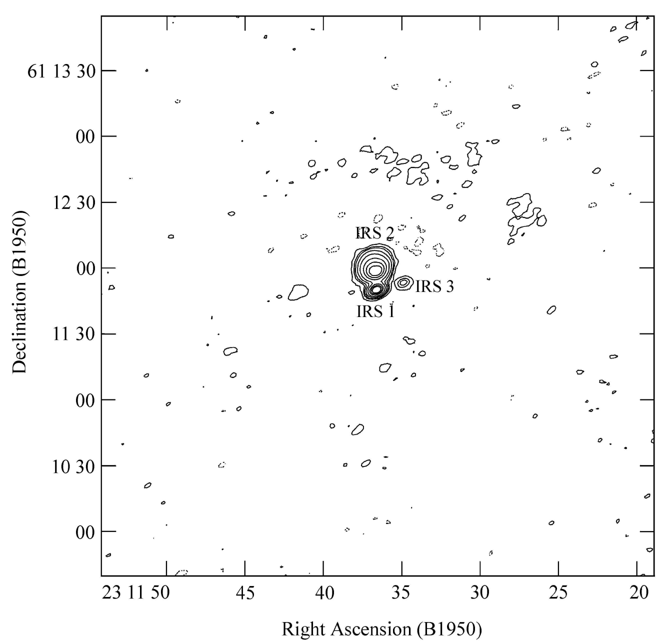

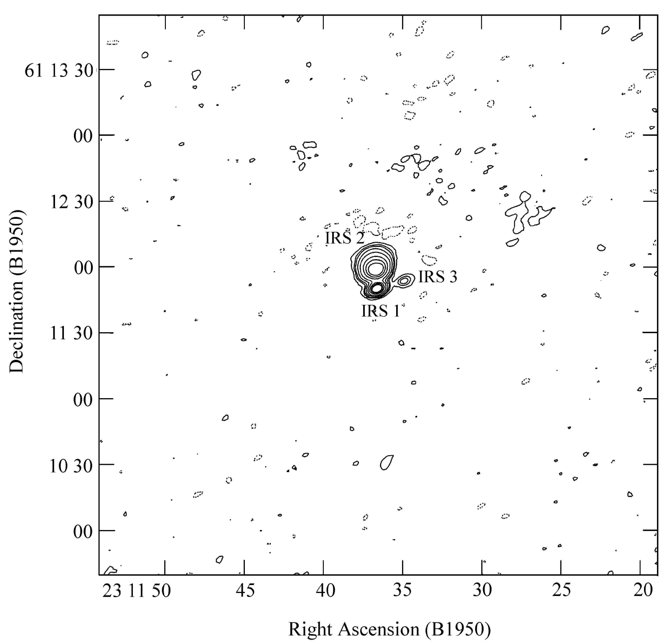

Fig. 3 Top: Continuum map associated with IRS 1–3 at 23.69 GHz. The contours for the continuum are plotted at –0.013, –0.008, –0.003, 0.03, 0.008, 0.013, 0.025, 0.051, 0.10, 0.15, and 0.21 Jy beam^{-1}. Bottom: Continuum map associated with IRS 1–3 at 23.72 GHz. The contours for the continuum are plotted at –0.011, –0.007, –0.002, 0.002, 0.007, 0.011, 0.022, 0.044, 0.089, 0.13, and 0.17 Jy beam^{-1}.

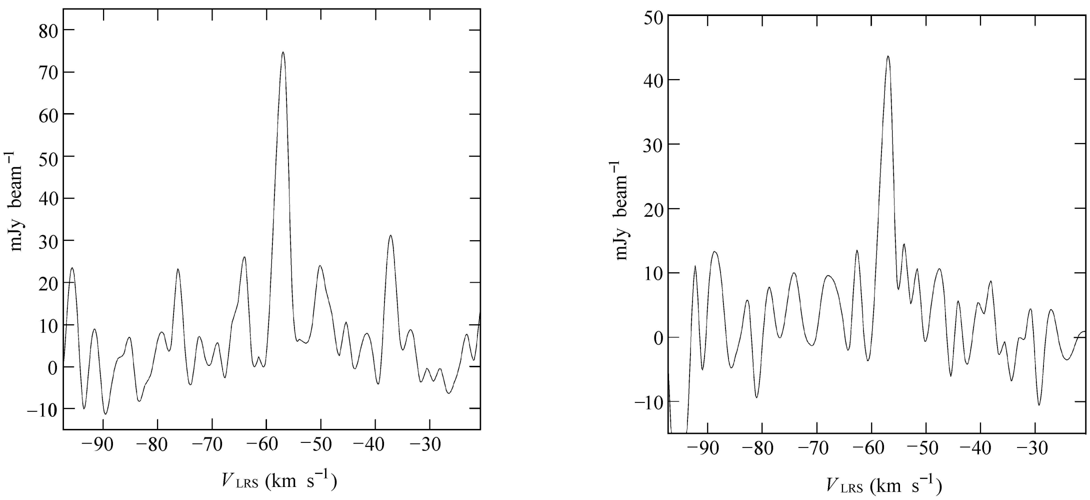

Fig. 4 Emission spectra of the (1, 1) line (left) and (2, 2) line (right) from the region A toward the HII region associated with IRS 1. The velocity resolution is 1.24 km s^{-1}. The rms noise is 7 mJy per beam.

The approach requires an assumption about the abundance [NH_3/H_2] ratio, which is the largest source of uncertainty of the method. The ratio has been estimated to be between 10^{-7} for small, dark clouds (Ungerechts, Walmsley & Winnewiser 1980) and 10^{-5} in dense nucleus of molecular cloud (Genzel et al. 1982). The high temperature of the hot cores certainly increases the evaporation of icy mantles, making the chemical formation process in the vicinity of UC HII regions different from that in cold dark clouds. Thus, the gas phase is expected to be enriched with mantle constituents such as NH_3, CH_3OH and H_2O although the precise amount of enrichment is difficult to estimate. The ammonia abundance [NH_3/H_2] ranges from 10^{-8} to 10^{-5} in the dense core of Orion-KL (Wiseman & Ho 1998). Assuming a [NH_3/H_2] ratio of 10^{-7} due to the low rotational temperature in the region marked A, we obtained $n \simeq 2.5 \times 10^5\,\mathrm{cm}^{-3}$ and $M \simeq 8\,M_\odot$. Figure 1 has shown that the NH_3 emission is very clumpy around the IRS 1 region, and these clumps are likely to have the same physical properties as those in region A with density of $\simeq 10^5\,\mathrm{cm}^{-3}$ and mass ranging from several to tens $M_\odot$. This is consistent with the results of HCN and HCO^+ maps (Pratap, Snyder & Batrla 1992).

2.2 Velocity Structure Around IRS 1

Because the hyperfine components of the (2, 2) lines are well separated by large splittings, the kinematics can be traced without confusion of line blending. We could obtain a (2, 2) absorption line width of ~ 6.8 km s^{-1} by a Gaussian fitting. Typical ammonia line width is about 3 km s^{-1} (Churchwell et al. 1990). Thermal broadening is too small to explain the observed line width. Even at the high kinetic temperature of hot cores, ~ 200 K, the thermal width is only ~ 0.7 km s^{-1}. Most likely, the broad line width is due to the presence of a systematic expanding or contracting motion.

We present the velocity structure around IRS 1 in the right ascension-velocity plot shown in Figure 5. At $8''$ resolution in space and 1.24 km s^{-1} in the velocity for the line (1, 1) we find that five absorption features of the main and the satellite components emerge and their peaks are easily distinguished. The line emission from the main and satellite components is systematically redshifted with respect to the absorption. We estimate a maximum redshift of 3.8 km s^{-1} (three spectral channels) for each component.

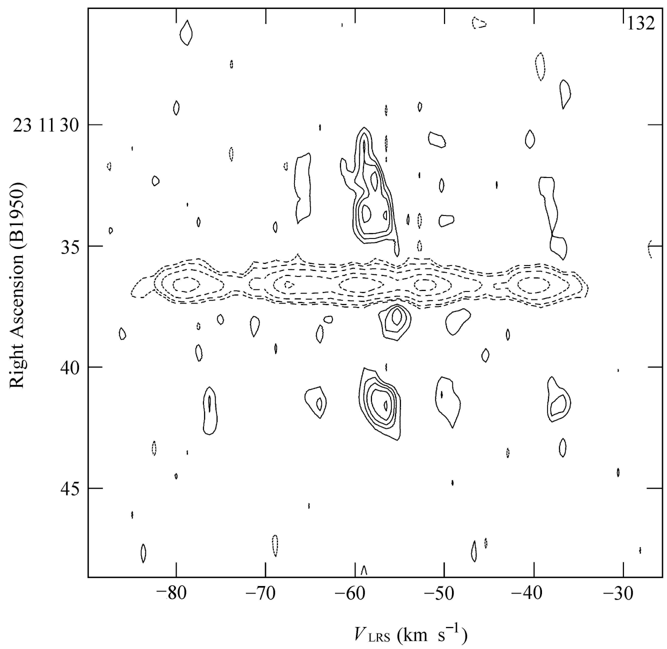

Fig. 5 Position-velocity plot of the NH_3 (1, 1) emission. The contours for the integrated emission are plotted at –0.19, –0.14, –0.095, –0.05, –0.025, –0.014, 0.014, 0.025, 0.033, and 0.05 Jy $beam^{-1}$.

In Figure 6 the NH_3 absorption is shown for selected velocity ranges in the blue and red line wings. NH_3 emission was only seen at the redshifted side ($V_{LSR} = -54.1$ to –56.5 km s^{-1}), while no blueshifted line wings were detected from –61.5 to –64.0 km s^{-1}. The orientation of the red lobe approximately agrees with the orientation of the CO red lobe mapped by Scoville et al. (1986) and Davis et al. (1998).

2.3 Discussion

The velocity-position (Figure 5) shows four arc-shaped or C-shaped structures visible in emission. These features can originate from the projection effects associated with a spherically expanding shell (Keto & Ho 1989). There is growing evidence that bipolar outflows is a basic component in the formation process of massive stars. In addition, massive stars have powerful winds which are expected to cause a considerable impact on their environment as they deposit momentum and mechanical energy into the interstellar medium. The interaction of the bipolar outflows and the stellar winds with the interstellar medium may produce a dense shell of circumstellar gas that expands away from the star, which may produce the observed expansion.

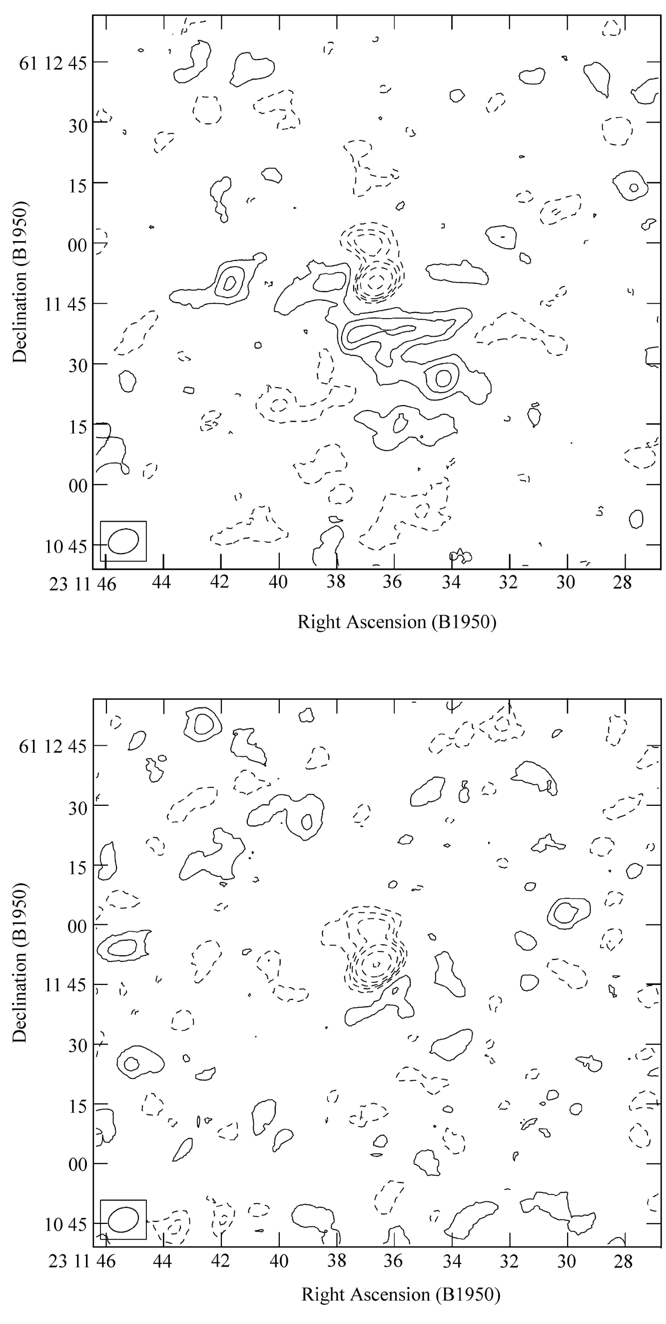

Fig. 6 Top: Contours of redshifted NH_3 emission from –54.1 to –56.5 km s^{-1}). The contours for the integrated emission are plotted at –0.5, –0.25, –0.13, –0.07, –0.05, –0.025, 0.025, and 0.05 Jy beam$^{-1}\times$ km s^{-1}. Bottom: Contours of blueshifted NH_3 emission from –61.5 to –64.0 km s^{-1}. The contours for the integrated emission are plotted at –0.28, –0.14, –0.085, –0.056, –0.028, 0.028, 0.056, and 0.085 Jy beam$^{-1}\times$ km s^{-1}.

The NH_3, and other molecular line emissions observed by Scoville et al. (1986), Davis et al. (1998) and Pratap, Snyder & Batrla (1992) indicated that on one hand, these high-density tracers have shown the presence of a cavity in the material around IRS 1 HII region, which could be a result of the expansion of the HII region possibly driven by both bipolar outflows and stellar wind. Although Pratap, Snyder & Batrla (1992) believed the presence of strong ^{13}CO emission in the cavity, we suggest that this may be a projection effect because high-density material is usually located in the innermost part of the cores, while less dense material is located further out. Observations have shown that the molecular hydrogen density has a centrally condensed structure (Zhang & Ho 1997). On the other hand, the direction of the expanding shell at first may be along a line from southeast to northwest and parallel to the axis of the bipolar CO outflow. Considering that IRS 2, the optical HII region NGC 7538, and IRS 3 are situated respectively $10''$, $30''$ north of, and $15''$ west of IRS 1, these massive stars produce powerful winds and outflows, which are expected to cause a considerable impact on the environment around IRS 1, especially in its north where most of the molecular gas would be dispersed. So, no high-density molecular lines are detected there because the gas density is too low to excite effectively high-density molecular lines, such as NH_3, HCN and HCO^+, while some lower density lines such as CO, could still be excited. Therefore, only the red lobe of NH_3 rather than a bipolar NH_3 outflow was detected, while CO emission exhibits a bipolar outflow.

To sum up, we can see: as a whole, the hot molecular core formed a spherical half-shell and was expanding away from the IRS 1 HII region, as the result of interaction of the bipolar outflows and the stellar winds with the ambient medium.

Acknowledgements We thank an anonymous referee for several helpful comments. This work was supported by the National Natural Science Foundation of China, under grant 19973017 and 10103003.

References

Churchwell E., Walmsley C. M., Cesaroni R., 1990, A&AS, 83, 119
Davis C. J., Moriarty-Schieven G., Eislöffel J. et al., 1998, AJ, 115, 1118
Dickel H. R., Rots A. H., Gross W. M. et al., 1982, MNRAS, 198, 256
Gaume R. A., Johnston K. J., Nguyen H. A. et al., 1991, ApJ, 376, 608
Genzel R., Downes D., Ho P. T. P., Bieging J., 1982, ApJ, 259, L103
Ho P. T. P., Haschick A. D., 1986, ApJ, 304, 501
Kameya O., Morita K.-I., Kawabe R., Ishiguro M., 1990, ApJ, 355, 562
Madden S. C., Irvine W. M., Matthews H. E. et al., 1986, ApJ, 300, L79
Menten K. M., Walmsley C. M., Henkel C., Wilson T. L., 1986, A&A, 157, 318
Pratap P., Snyder L. E., Batrla W., 1992, ApJ, 387, 241
Rots A. H., Dickel H. R., Forster J. R. et al., 1981, ApJ, 245, L15
Scoville N. Z., Sargent A. I., Sanders D. B. et al., 1986, ApJ, 303, 416
Ungerechts H., Walmsley C. M., Winnewiser G., 1980, A&A, 88, 259
Wilson T. L., Bieging J., Downes D., 1978, A&A, 63, 1
Wiseman J. J., Ho P. T. P., 1998, ApJ, 502, 676
Zhang Q., Ho P. T. P., 1997, ApJ, 488, 241
Zheng X., Zhang Q., Ho P. T. P., Pratap P., 2001, ApJ, 550, 301